Hindawi
Journal of Advanced Transportation
Volume 2022, Article ID 6342857, 15 pages
https://doi.org/10.1155/2022/6342857

Research Article

Variable Cell Transmission Model for Mixed Traffic Flow with Connected Automated Vehicles and Human-Driven Vehicles

Yuting Jin,[1,2] Zhihong Yao ,[1,2,3] Jiazhe Han,[1,2] Lu Hu,[1,2,3] and Yangsheng Jiang[1,2,3]

[1]*School of Transportation and Logistics, Southwest Jiaotong University, Chengdu, Sichuan 610031, China*
[2]*National Engineering Laboratory of Integrated Transportation Big Data Application Technology, Southwest Jiaotong University, Chengdu, Sichuan 611756, China*
[3]*National United Engineering Laboratory of Integrated and Intelligent Transportation, Southwest Jiaotong University, Chengdu, Sichuan 611756, China*

Correspondence should be addressed to Zhihong Yao; zhyao@swjtu.edu.cn

Received 7 March 2022; Revised 20 March 2022; Accepted 24 March 2022; Published 12 April 2022

Academic Editor: Yang Yang

The current research on the mixed traffic flow characteristics of human-driven vehicles (HDVs) and connected automated vehicles (CAVs) mainly focuses on the micro-level. To study the characteristics of the mixed traffic flow from the medium and macro level, this paper proposes a variable cell transmission model (VCTM). First, the fundamental diagram is introduced based on the phenomena of hysteresis of traffic flow. Second, the VCTM with different market penetration rates (MPR) of CAVs is proposed based on the classical cell transmission model (CTM). Then, the effectiveness of VCTM is verified by micro-simulation based on the intelligent driver model (IDM). Finally, some congestion indexes are selected to discuss the characteristics of mixed traffic flow based on the VCTM with an expressway simulation. The results show that the traffic capacity and congestion dissipation capacity gradually are increased with the increase of MPR of CAVs. The homogeneous CAVs traffic flow capacity can reach 1.41 times that of the homogeneous HDVs traffic flow, and the congestion dissipation time can be reduced by 25%. The larger MPR is, the greater the improvement effect is. In addition, compared with CTM, VCTM can reflect the delay, queuing, and dissipation of mixed traffic flow more accurately, which is helpful to capture the evolution mechanism of mixed traffic flow in the future.

1. Introduction

In recent years, the rapid development of automatic driving and communication technology enabled the large-scale application of CAVs. The intelligent transportation system with CAVs has attracted the increasing attention of scholars [1]. Nevertheless, the popularity of CAVs takes a specific time; there will be a mixed traffic flow composed of CAVs and HDVs for a long time in the future. Therefore, it is of great significance to study the traffic characteristics and propagation mechanism of mixed traffic flow. In real-time management and control of traffic flow, many studies have been applied modeling and simulation of mixed traffic flow with CAVs. These studies can be divided into two categories: one focuses on theoretical analysis [2–4] and the other on simulation analysis [5–7]. This work mainly focuses on the second part, i.e., simulation analysis.

Against such a background, to gain the basic characteristics of general traffic flow, the homogeneous HDVs traffic flow environment is studied at the macro level at first. Daganzo [8, 9] discretized LWR (Lighthill-Whitham Richards) model to obtain the Cell Transmission Model (CTM). Compared with higher order traffic flow models [10], CTM is a first-order model, which is widely applied in traffic simulation [11], traffic distribution [12], and traffic signal control [13] because of the low requirement of calculation. Then, many scholars have focused on making corresponding improvements on the CTM for different study scenarios, such as city roads, expressways, intersections, and air transportation. To predict the traffic flow accurately, Tiaprasert et al. [14] and Szeto et al. [15] proposed a multiclass CTM and a real-time traffic control method, respectively. Carlos and Ferrara [16] studied the optimal speed control design of loop traffic based on the

variable-length CTM (VLM) to optimize the travel time. Zhang et al. [17] studied the impact of traffic demand of the target road network on the overall progress of congestion evacuation based on the CTM and the macroscopic fundamental diagram (MFD). Results showed that the model could improve the computational efficiency of the dynamic traffic assignment model. Shirke et al. [18] proposed an arterial CTM (ACTM) to capture the congestion and overflow of turning lanes in the arterial traffic network. Compared with the classical CTM, ACTM can improve the accuracy of queue estimation by 20%~80%. Dong et al. [19] developed an improved CTM to predict the duration of traffic congestion and estimate the spatial diffusion law of congestion. Moreover, an asymmetric CTM based on the upper limit of ramp flow rate and queue length was proposed to achieve the optimal control of on-ramp flow by Gomes and Horowitz [20]. For unsignalized intersections, Flötteröd and Rohde [21] studied an incremental node model (INM) to solve the problem of priority allocation based on the incremental transfer principle of the CTM. For signalized intersections, Srivastava [22] and Gao et al. [23] estimated the capacity of intersections based on the CTM with a new demand function and the Enhanced-CTM, respectively. Furthermore, according to the CTM and the fundamental diagram model, Lo [24] proposed a dynamic traffic control equation to predict traffic conditions and demand patterns. In traffic signal optimization, Lin and Wang [25] developed an improved mixed-integer linear programming model to obtain the optimal signal sequence based on CTM, which is used to capture the signal priority of vehicles at intersections.

However, as previously mentioned, the studies are based on HDVs to expand the CTM, without considering the impact of CAVs. At present, wireless communication and automatic driving technology promote the development of CAVs. The application of CAVs will significantly improve traffic efficiency and safety [26–28]. The large-scale application needs the support of related infrastructure such as intelligent roads. However, the upgrading of smart road infrastructure is a long process. Consequently, the transition period from homogeneous HDVs to homogeneous CAVs is long [29]. To analyze the characteristics of the mixed traffic flow composed of CAVs and HDVs has attracted a great deal of attention. According to the traffic flow theory, Levin and Boyles [30] established a multilane CTM to study the optimization algorithm for lane direction decision-making of CAVs. The results showed that the proposed heuristic algorithm could reduce the travel time of the traffic system, but they only focused on the traffic flow characteristics in the homogeneous CAVs environment. Based on the fundamental diagram of mixed traffic flow, Qin and Wang [31] proposed a CTM for mixed traffic flow with different MPR of CAVs. Results showed that the degree of queue length and dissipation time decreased with the MPR of CAVs. Whereas they did not consider the limitation of the CTM (e.g., the equal).

To sum up, the current researches inspire us to focus on the following three gaps: (1) most of the existing research uses microscopic models to capture the driving behavior of vehicles and describe the propagation mechanism of traffic flow. However, there are many parameters of the microscopic model that must be calibrated by collecting many data. In addition, compared with the meso and macro models, the micro model has low efficiency with much calculation. Therefore, using the macro CTM will reduce the complexity of the simulation model and improve the simulation efficiency. (2) Most CTM models only study the characteristics of homogeneous traffic flow (e.g., HDVs or CAVs). With the development of CAVs, there will be a mixed traffic flow composed of CAVs and HDVs in the future. (3) In some studies of mixed traffic flow, they did not break through the limitation of equal cell length of the CTM. What is more, its basic assumption is that the traffic flow obeys the triangle fundamental diagram, and the hysteresis phenomenon is not considered. It is impossible to accurately describe the relationship between traffic volume and density under congestion, and the results of the study are far from the actual situation. Moreover, based on the three-phase traffic flow theory, the volume-density-speed of traffic flow is not an ideal triangular relationship. There is a substable region, which presents a converse 'λ' shape. When traffic density is greater than the critical density, there will be 'ghost jam'. Therefore, it is more realistic to propose a VCTM to describe the characteristics of mixed traffic flow considering the hysteresis phenomenon.

To fill in these gaps, this study proposes a VCTM for mixed traffic flow with CAVs and HDVs. The main contributions of this work can be summarized as follows:

(1) The VCTM is proposed based on "λ" shape fundamental diagram of mixed traffic flow to consider the cell density and cell length simultaneously

(2) A microscopic simulation is designed to verify the effectiveness of the VCTM in SUMO based on IDM car-following model

(3) Some congestion indexes, such as travel speed, delay, and congestion scale, are selected to discuss the characteristics of mixed traffic flow based on the VCTM

The remainder of this paper is organized as follows. Section 2 proposes the VCTM based on the classical CTM and the CTM for mixed traffic flow. The validity of the VCTM is verified by SUMO simulation, and the applicability of CTM and VCTM is presented in Section 3. Section 4 analyzes the relationship between the time-space change of traffic flow and the MPR of CAVs. Finally, the conclusions and future works are summarized in Section 5.

2. Cell Transition Model

2.1. Classical Cell Transition Model. To realize the macro dynamic traffic control of expressway, alleviate congestion, and improve traffic capacity. Daganzo [8, 9] proposed the classical cell transition model. Moreover, the transmission relationship between cells is a trapezoidal function based on traffic flow and density, as shown in Figure 1. The traffic flow at any time can be calculated by

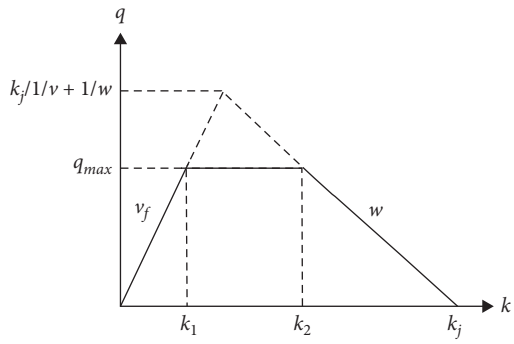

Figure 1: Flow density diagram in CTM.

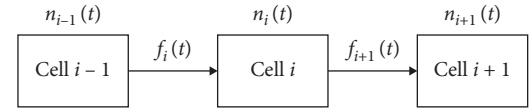

Figure 2: Schematic diagram of the basic road link of the CTM.

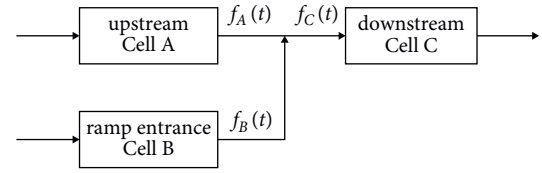

Figure 3: Schematic diagram of the merge road link of CTM.

$$q = \min\{v_f k, q_{\max}, w(k_j - k)\}, \tag{1}$$

where q is the traffic flow, $q_{\max}$ is the maximum traffic flow, w is the reverse wave speed, v_f is the free-flow speed, k is the traffic density, k_j is the congestion density, and k_1 and k_2 are the minimum and maximum traffic density, respectively.

2.1.1. Basic Link. From Figure 2, the number of vehicles in cell i at time t can be expressed as equation (2), and $f_i(t)$ is the number of vehicles entering cell i at time t, which can be calculated by

$$n_i(t+1) = n_i(t) + f_i(t) - f_{i+1}(t), \tag{2}$$

$$f_i(t) = \min\left\{n_{i-1}(t), Q_i(t), -\frac{w}{v_f}\left[N_i(t) - n_i(t)\right]\right\}, \tag{3}$$

where $n_i(t)$ is the number of vehicles in cell i at time t, $Q_i(t)$ is the maximum flow of cell i at time t, and$N_i(t)$ is the maximum number of vehicles that cell i can hold at time t.

These two capability parameters can describe the number of vehicles that can be sent and received by cell i at time t, which is defined in equations (4) and (5). Then, (2) can be simplified to equation (6).

$$S_i(t) = \min\{n_i(t), Q_{i+1}(t)\}, \tag{4}$$

$$R_i(t) = \min\left\{Q_i(t), -\frac{w}{v_f}\left[N_i(t) - n_i(t)\right]\right\}, \tag{5}$$

$$f_i(t) = \min\{S_{i-1}(t), R_i(t)\}. \tag{6}$$

Therefore, the traffic flow characteristics of the basic link of CTM can be described by equations (2)–(6).

2.1.2. Merging Link. After satisfying the transport constraints between cells in Figure 3, considering the receiving vehicles of cell C limit the transmission vehicles of cells A and B, the diverging model can be divided into two cases.

(1) When $S_A(t) + S_B(t) \le R_C(t)$,

$$\begin{cases} f_A(t) = S_A(t), \\ f_B(t) = S_B(t), \\ f_C(t) = f_A(t) + f_B(t). \end{cases} \tag{7}$$

(2) When $S_A(t) + S_B(t) > R_C(t)$, considering the priority of merging, the merging coefficients $\alpha_A(t)$ and $\beta_A(t)$ need to be introduced here.

$$\begin{cases} f_A(t) = \text{mid}\{S_A(t), R_C(t) - S_B(t), \alpha_A(t)R_C(t)\}, \\ f_B(t) = \text{mid}\{S_B(t), R_C(t) - S_A(t), \alpha_B(t)R_C(t)\}, \\ f_C(t) = f_A(t) + f_B(t) = R_C(t), \\ \alpha_A(t)) + \alpha_B(t) = 1. \end{cases} \tag{8}$$

Therefore, equations (2), (6)–(8) can be used to describe the traffic flow characteristics of the CTM merging link.

2.1.3. Diverging Link. The receiving vehicles of cells F and G limit the transmission vehicles to two cells when cell E diverges, as shown in Figure 4. The diverging coefficient $\beta_F(t)$ and $\beta_G(t)$ is introduced to consider a diverging priority.

$$\begin{cases} f_E(t) = \min\left\{S_E(t), \dfrac{R_F(t)}{\beta_F(t)}, \dfrac{R_G(t)}{\beta_G(t)}\right\}, \\ f_F(t) = \beta_F(t) f_E(t), \\ f_G(t) = \beta_G(t) f_E(t), \\ \beta_F(t) + \beta_G(t) = 1. \end{cases} \tag{9}$$

Therefore, equations (2), (6), and (9) can be used to describe the traffic flow characteristics of the CTM diverging link.

2.2. Car-Following Modes of Mixed Traffic Flow. The mixed traffic flow is composed of HDVs and CAVs. There are three car-following modes based on vehicle-to-vehicle (V2V) communication conditions [32]. As shown in Figure 5(a), if the current and the following vehicle are CAVs, it can be described as a cooperative adaptive cruise control (CACC) mode. As shown in Figure 5(b), if the current vehicle is an

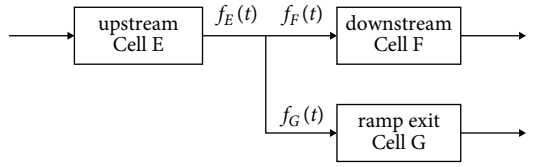

Figure 4: Schematic diagram of diverge road section of CTM.

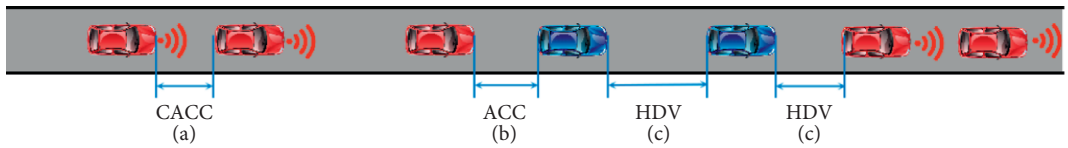

Figure 5: Car following modes of mixed traffic flow. (a) CACC, (b) ACC, and (c) HDV.

HDV, the following car is a CAV. Because the HDV lacks network communication equipment, the CAV cannot drive cooperatively with it, resulting in CACC vehicles degradation in the mixed traffic flow [28]. Moreover, it can be described as adaptive cruise control (ACC) mode. In addition, if the current vehicle is an HDV or CAV, and the following vehicle is HDV, as shown in Figure 5(c).

$$\begin{cases} p_{\mathrm{CACC}} = p^2, \\ p_{\mathrm{ACC}} = p(1-p), \\ p_{\mathrm{HDV}} = 1-p. \end{cases} \tag{10}$$

In Figure 5(c), it can be described as a human-driven mode (HDV). Therefore, if the platoon intensity is not considered [33], that is, the random distribution of CAVs and HDVs. The MPR of CAVs in mixed traffic flow is p, the proportion of different car-following modes in mixed traffic flow can be obtained by equation (15).where p_{CACC}, p_{ACC}, and p_{HDV} are the proportion of CACC, ACC, and HDV car-following mode, respectively.

2.3. The CTM for Mixed Traffic Flow. In order to facilitate the derivation of the fundamental diagram, the lane-changing behavior of vehicles is not considered. The relationship between traffic volume, density, and speed in mixed traffic flow can be deduced based on related research [15, 17, 34].

$$k = \frac{1}{\sum_{m=1}^{M} p_m\left(\mathrm{vT}_m + d_m\right)}, \tag{11}$$

$$v = \frac{1}{k\sum_{m=1}^{M}\left(p_m T_m\right)} - \frac{\sum_{m=1}^{M}\left(p_m d_m\right)}{\sum_{m=1}^{M}\left(p_m T_m\right)}, \tag{12}$$

$$q = \frac{1}{\sum_{m=1}^{M}\left(p_m T_m\right)} - k\frac{\sum_{m=1}^{M}\left(p_m d_m\right)}{\sum_{m=1}^{M}\left(p_m T_m\right)}, \tag{13}$$

where M is the type of car-following modes; in this study, the M is 3, which means CACC, ACC, and HDV. p_m is the proportion of the mth car-following mode of mixed traffic flow, v is the equilibrium speed, T_m is the headway of vehicles in mth car-following mode, and d_m is the minimum headway of vehicles in mth car-following mode. Moreover, when the velocity is free-flow speed, the $q_{\max}$ corresponding critical density k_c can be deduced in equations (14) and (15) based on equation (11).

$$k_c = \frac{1}{\sum_{m=1}^{M} p_m\left(v_f T_m + d_m\right)}. \tag{14}$$

The maximum traffic volume is

$$q_{\max} = \frac{v_f}{\sum_{m=1}^{M} p_m\left(v_f T_m + d_m\right)}, \tag{15}$$

where the speed is 0, the congestion density is

$$k_j = \frac{1}{\sum_{m=1}^{M} p_m d_m}. \tag{16}$$

Therefore, the fundamental diagram of mixed traffic flow can be obtained by equations (14)–(16). From Figure 6, the reverse wave speed and speed of the mixed traffic flow can be calculated by

$$w = -\frac{\sum_{m=1}^{M} p_m d_m}{\sum_{m=1}^{M} p_m T_m}. \tag{17}$$

$$v = \min\left\{v_f, \frac{q_{\max}}{k_i}, -\frac{w\left(k_j - k_i\right)}{k_i}\right\}. \tag{18}$$

Then, equation (19) can be obtained by taking equations (15)–(17) into equation (18).

$$v = \min\left\{v_f, \frac{v_f}{k\sum_{m=1}^{M} p_m\left(v_f T_m + d_m\right)}, \frac{\sum_{m=1}^{M} p_m d_m}{\sum_{m=1}^{M} p_m T_m}\left(\frac{1}{k\sum_{m=1}^{M} p_m d_m} - 1\right)\right\}. \tag{19}$$

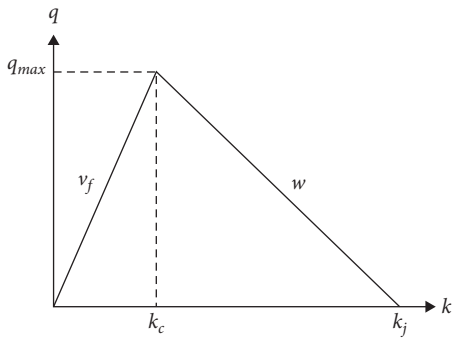

Figure 6: Fundamental diagram of mixed traffic flow.

Therefore, the cell transmission flow and the number of vehicles in cell i at time t can be calculated by equations (20)-(21).

$$f_i(t) = \min\left\{n_{i-1}(t), Q_{\max}, -\frac{v}{v_f}\left[N_i(t) - n_i(t)\right]\right\}, \quad (20)$$

$$n_i(t + \Delta t) = n_i(t) + f_i(t) - f_{i+1}(t). \quad (21)$$

2.4. Analysis of Fundamental Diagram of Mixed Traffic Flow. The volume, density, and speed of mixed traffic flow are related to the MPR of CAVs based on equation (19). In particular, refer to [3, 35], the parameters setting of different car-following modes are shown in Table 1. In addition, the MPR are set as 0, 0.2, 0.4, 0.6, 0.8, and 1, respectively. Then, the fundamental diagram of mixed traffic flow can be obtained, as shown in Figure 7.

Figure 7 represents that traffic capacity increases with the MPR of CAVs, and the growth is more visible when the MPR is within 0.6 to 1. This indicates that the traffic capacity of mixed traffic flow is positively correlated with the MPR of CAVs. Further analysis shows that when the MPR increases, the number of CACC and ACC increases gradually, and many vehicles can realize V2V real-time communication. In this scenario, when the leader vehicles suddenly change their driving behavior, the following vehicle can take reasonable countermeasures quickly. Therefore, the traffic capacity of mixed traffic flow can be improved by maintaining a small headway.

Moreover, when the MPR is 1, the mixed traffic flow can be regarded as homogeneous CAVs traffic flow. In this case, CAVs realize cooperative driving through intelligent sensor devices. Currently, the cell transmission capacity and road traffic capacity reach the maximum. This means that the large-scale use of CAVs is conducive to improving traffic efficiency, thus reducing delay and congestion, and improving traffic flow performance.

2.5. VCTM Based on Mixed Traffic Flow. The actual traffic link length is not equal, and the classical CTM is used to divide the road link into isometric cells, which may not accurately describe the characteristics of mixed traffic flow. Furthermore, the division standard is the product of the

Table 1: The parameters setting of different car-following modes.

Car-following modes	T_m (s)	d_m (m)
CACC	1.0	7.0
ACC	1.2	7.0
HDV	1.5	7.0

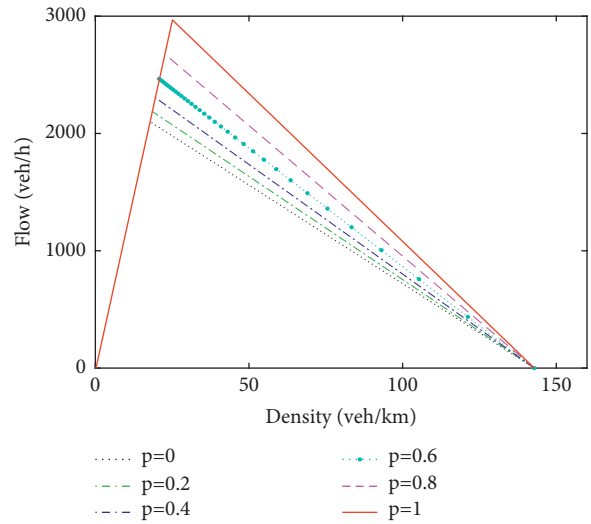

Figure 7: Fundamental diagram of mixed traffic flow under different MPR of CAVs.

simulation step length and the free-flow velocity. When the length of the road section cannot be divided equally by the cells, as shown in Figure 8, the method of reducing the simulation step length is usually adopted. However, this method will reduce the simulation efficiency and is not conducive to CTM's simulation of large-scale transportation networks. To solve this problem, the VCTM is proposed. The VCTM should meet the requirements, $x_i \geq v_f \Delta t$, that is, the length of the cell is not less than the distance the vehicle passes through in time at free-flow speed. Based on the assumption of uniform distribution of vehicles in the same cell, that is, the traffic density in the cell is evenly distributed [8, 9, 36], the sending capacity $S_i(t)$ and receiving capacity $R_i(t)$ of cell i are defined by Equations (22)-(23).

$$S_i(t) = \min\left\{\frac{x}{x_i} n_i(t), Q_{i+1}(t)\right\}. \quad (22)$$

$$R_i(t) = \min\left\{Q_i(t), -\frac{x}{x_i}\left(\frac{w}{v_f}\right)\left[N_i(t) - n_i(t)\right]\right\}. \quad (23)$$

Both sides of Equations (22) and (23) are divided by Δt:

$$S_i(t) = \min\left\{v_f k_i(t), q_{i+1}^{\max}(t)\right\}. \quad (24)$$

$$R_i(t) = \min\left\{q_i^{\max}(t), -w\left[k_i^j(t) - k_i(t)\right]\right\}, \quad (25)$$

where $q_{i+1}^{\max}(t)$ is the maximum flow of cell $i+1$ at time t, and $k_i^j(t)$ is the congestion density of cell i at time t, j is the jam state.

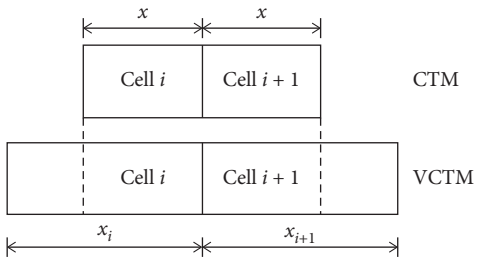

Figure 8: Cell diagram of CTM and VCTM.

In CTM, the cell length is fixed and equal, and the number of cell vehicles is used to represent the cell state. However, the cell length changes in VCTM, and the traffic density is used to describe the cell state.

$$k_i(t+1) = k_i(t) + \frac{\Delta t}{x_i}\left[q_i(t) - q_{i+1}(t)\right], \tag{26}$$

where $k_i(t+1)$ is the traffic density of cell i at time t.

Based on the three-phase traffic flow theory [37], there is a substable region in the actual traffic flow. When the density is greater than the critical density, 'ghost jam' will occur. Therefore, the traditional triangle fundamental diagram is improved to consider the influence of the hysteresis phenomenon, as shown in Figure 9. It can capture the actual traffic flow characteristics more accurately.

Figure 9 shows that when the free-flow direction changes to the congested flow, the traffic flow density is k_1, and when the congestion density changes to the free flow, the traffic flow density is k_2, and $k_1 < k_2$.

$$\begin{cases} k_1 = -k_j \dfrac{w}{v_f + w}, \\ \\ k_2 = \dfrac{q_{\max}}{v_f}. \end{cases} \tag{27}$$

For better understanding, we introduce a parameter $\varphi_i(t)$, which is defined as the traffic state of cell i at time t. When $\varphi_i(t) = 0$, it means that cell i is free-flow at time t, and when $\varphi_i(t) = 1$, it means that it is congested flow at time t.

$$\varphi_i(t) = \begin{cases} 0, & \text{if } k_i(t) \le k_1, \\ 1, & \text{if } k_i(t) \ge k_2, \\ \varphi_i(t-1), & \text{otherwise.} \end{cases} \tag{28}$$

It is easy to know that the sending capacity of a cell is determined by the traffic density of the upstream cell and the outflow capacity of the downstream cell. The receiving capacity of the cell is mainly determined by the traffic state of the cell. Therefore, the expressions of cell transmitting and receiving ability can be obtained by Equations (29)-(30).

$$S_i(t) = \min\left\{v_f k_i(t), q_{i+1}^{\max}(t)\right\}. \tag{29}$$

$$R_i(t) = q_i^{\max}(t)\left[1 - \varphi(t)\right] + w\varphi(t)\left[k_i^j(t) - k_i(t)\right]. \tag{30}$$

Then, equations (24), (28)–(30) can be used to describe the traffic flow characteristics of the VCTM in the basic link, and the merging and diverging link models remain unchanged.

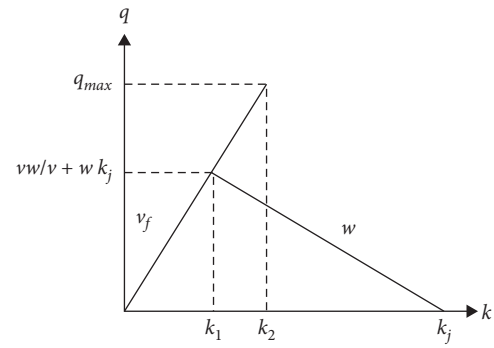

Figure 9: The fundamental diagram with hysteresis.

3. Model Validation

The existing vehicle trajectory data are HDVs, such as NGSIM [38] and pNEUMA [39] databases. The trajectory data of CAVs are lacking in these databases. The mixed traffic flow studied in this work is composed of HDVs and CAVs, and these databases cannot be used to calibrate the proposed model. Instead, the driving behavior of CAVs is easy to implement in micro-simulation software [40]; thus, this section verifies the validity of the proposed model based on micro-simulation software.

3.1. VCTM Simulation. Due to the frequent and serious consequences that arise from expressway traffic crashes, we focus on capturing the characteristics of expressway traffic flow [41]. The basic link of the expressway with a total length of 4500 m is selected as the simulation segment. The segment is divided into 30 cells with different lengths based on the method proposed by Hu et al. [42], as shown in Figure 10. The simulation time step is 3 s, the simulation time is 1200 s, the free-flow velocity is 33.3 m/s, and the input flow is 1200 veh/h. There is a traffic accident in the 18th cell at 300 s, which leads the output capacity to be reduced to 0 veh/h. Therefore, this accident caused a large area of traffic congestion. Then, the accident treatment is completed at 600 s, and the congested vehicles begin to evacuate. In addition, the MPR of CAVs are set as 0, 0.2, 0.4, 0.6, 0.8, and 1, respectively. The macro numerical simulation experiment is carried out by MATLAB, and the change of traffic density of each cell with time and space is obtained, as shown in Figure 11.

Figure 11 shows that after the traffic accident at the 18th cell at 300 s, the traffic density of the cell increases rapidly; the former cell starts to queue and waits until the traffic accident is cleared. From 600 s, the congestion begins to dissipate, the vehicle returns to a normal state, and the cell density decreases gradually. From Figure 11, the queue propagates to the 8th cell and the queue dissipation time needs 912 s when p is 0. When p is 1, the queue propagates only to the 10th cell and the queue dissipation time only takes 741 s. This indicates that the larger the MPR of CAVs is,

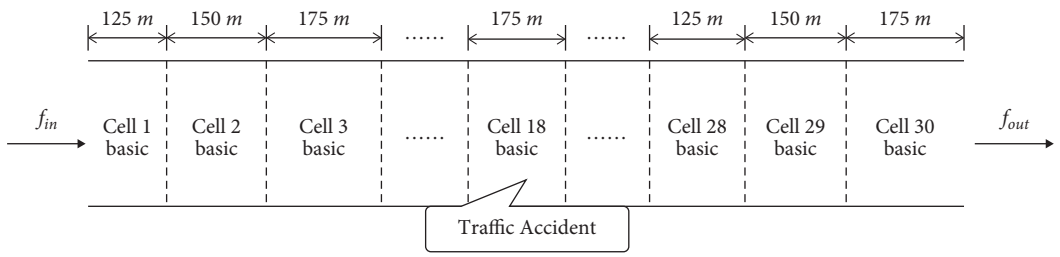

Figure 10: Mixed traffic flow simulation link.

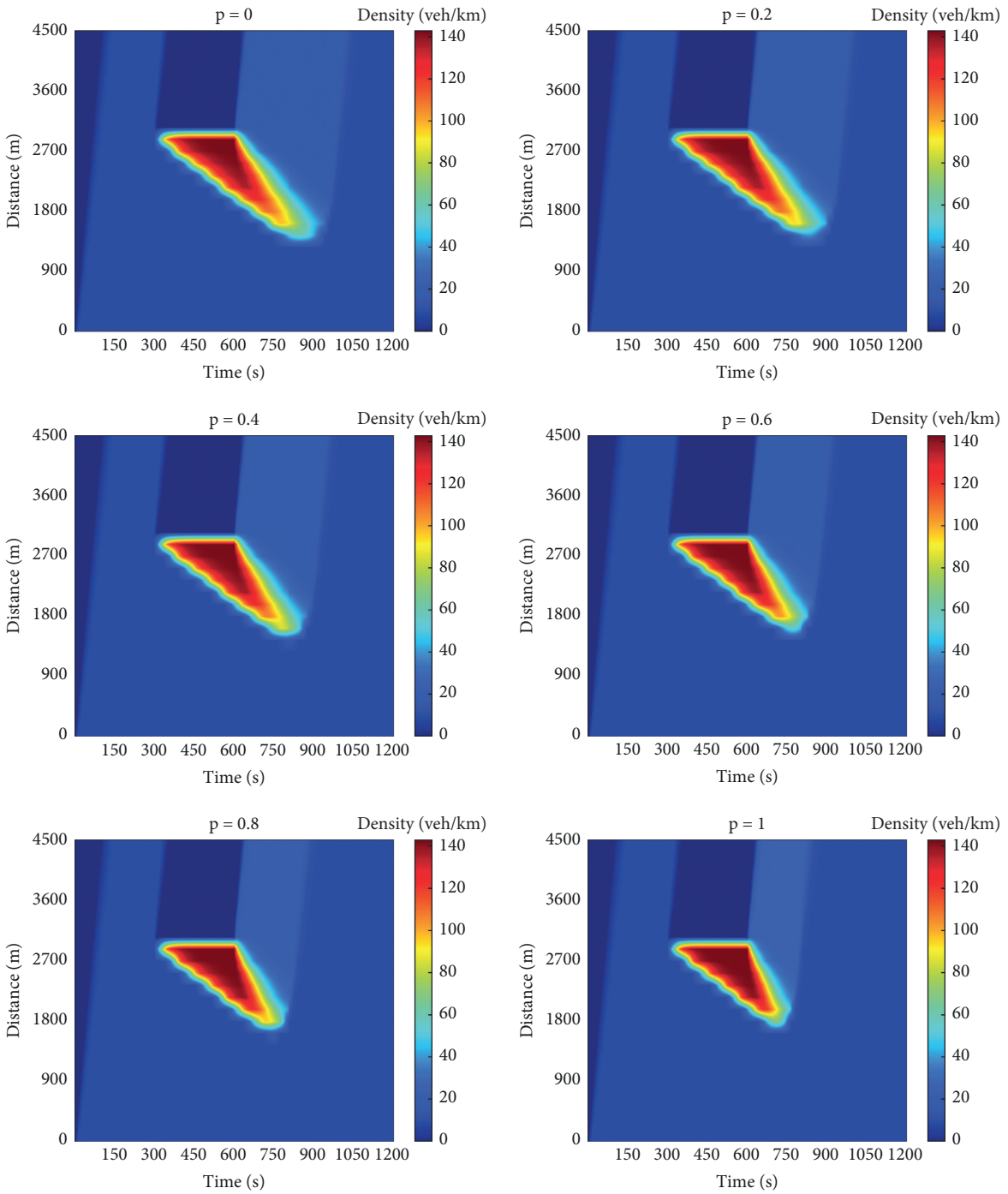

Figure 11: Density variation of VCTM.

the fewer congestion cells and the shorter the queue dissipation time are. Moreover, the 23.08% reduction of queuing dissipation time of homogeneous CAVs traffic flow than that of homogeneous HDVs. This is because when the MPR is low, there are many HDVs in mixed traffic flow, which cannot realize V2V communication. The headway in the VCTM is adopted with a more significant value to prevent collision between two adjacent vehicles. The more significant headway leads to the delay in transmitting more cells, so the queue dissipation time is longer. When the MPR is high, the number of vehicles accommodated by the cell increases with minor headway. Then, the number of delay cells decreases, and the queuing dissipation time is shorter. This indicates that the capacity of road congestion dissipation increases with the MPR of CAVs.

3.2. Microsimulation. To verify the effectiveness of the macro VCTM, the micro-simulation of mixed traffic flow in Section 3.1 is carried out. Then, the results are compared with the numerical simulation results of the VCTM.

More recently, to accurately describe the car-following behavior of mixed traffic flow, many scholars have used different car-following models to study the characteristics of traffic flow from multiple perspectives at the microlevel, such as intelligent driver model (IDM) [43], adaptive cruise control (ACC) model [44], and cooperative adaptive cruise control (CACC) model [45]. On the basis, the stability and safety of mixed traffic flow are analyzed. In terms of stability, Wang et al. [46] use the CACC model and ACC model to describe the car-following behavior of CAVs with connected communication and connected degradation, respectively, while for HDV, the IDM is used to reflect the car-following behavior. Then, it is found that the degradation of the CAVs leads to the decreasing of flow stability remarkably. In terms of safety, Yao et al. [28] also used the CACC model, ACC model, and IDM to describe the car-following behavior in mixed traffic flow. Furthermore, further analyzed the safety of mixed traffic flow by using indicators such as standard deviation of vehicle speed (SD), time exposed rear-end crash risk (TER), exposed time-to-collision (TET), and integrated time-to-collision (TIT).

To sum up, no matter to analysis the stability or safety of mixed traffic flow, most of the existing studies use different car-following models to describe the car-following behavior between CAVs and HDVs. Whereas, there are significant differences in the car-following mechanism and expression between different car-following models, in practical application. In addition, the differences will make human drivers feel strange and inadaptable. What is more, according to the research [47, 48], the unified car-following model with deep human imitation is more conducive to simulating the real traffic flow. In other words, using the same car-following model to describe the car-following behavior of CAVs and HDVs will be more matched with the driving habits of human drivers. Therefore, in this study, IDM with different MPR is used to describe the car-following behavior of CAVs and HDVs. Its equation will be presented as

$$a_{\mathrm{IDM}} = a\left[1 - \left(\left(\frac{v}{v_f}\right)^{\delta} - \left(\frac{S_0 + vT_m + v\Delta v/2\sqrt{\mathrm{ab}}}{h_m - L}\right)^2\right)\right], \quad (31)$$

where a is the maximum acceleration, b is the comfortable deceleration, v is the speed of the rear vehicle, v_f is the free-flow speed, Δv is the speed difference between the front and the rear vehicle, δ is the acceleration index, and its value is 4, S_0 is the minimum distance of the vehicle, and its value is 2 m, T_m is the safe headway of vehicles in m-th car-following mode (the value as shown in Table 1), and h_m is the headway of vehicles in m-th car-following mode, L is the length of the vehicle, and its value is 5 m.

The basic link of the expressway with a total length of 4500 m is selected as the simulation segment, which is divided into 30 cells with different lengths, as shown in Figure 10. The simulation parameter setting is consistent with Section 3.1. The microscopic simulation experiment is carried out by SUMO, and the change of traffic density of each cell with time and space is obtained, as shown in Figure 12.

Figures 11 and 12 show that the results of macro VCTM simulation are consistent with those of micro-simulation. With the increase of MPR of CAVs, the queue dissipation time decreases gradually. The ability to alleviate congestion is also improved.

3.3. CTM Simulation. In order to compare the applicability of VCTM and CTM models, the equal length simulation section is selected, which is divided into 45 links with equal lengths, as shown in Figure 13. The simulation parameter setting is consistent with Section 3.1. The numerical simulation experiment is carried out by MATLAB, and the change of traffic density of each cell with time and space is obtained, as shown in Figure 14.

Comparing Figure 14 with Figures 11 and 12, the overall trend is roughly the same; that is, with the increase of MPR of CAVs, the queue dissipation time gradually decreases.

3.4. Comparison of Results. To quantitatively describe the difference between CTM, VCTM, and microscopic simulation, the queue dissipation time is selected as the analysis index to calculate mean absolute error (MAE) and mean absolute percentage error (MAPE). The results are shown in Table 2.

Table 2 shows that with the increase of the MPR of CAVs, the congestion dissipation time decreases gradually. According to the error results in Table 2, compared with the microscopic simulation results, the errors of the two models are minimal. The maximum value of MAE of the CTM was 34 s, and the maximum value of MAPE was 4.18%. Moreover, the maximum value of MAE of VCTM was no more than 22 s, and the maximum value of MAPE of VCTM was 2.82%. Therefore, compared with CTM, the error of VCTM is smaller, the average error is reduced by 0.85%, and the relative error is reduced about two times. This means that the VCTM can accurately describe the characteristics of mixed traffic flow in the actual situation.

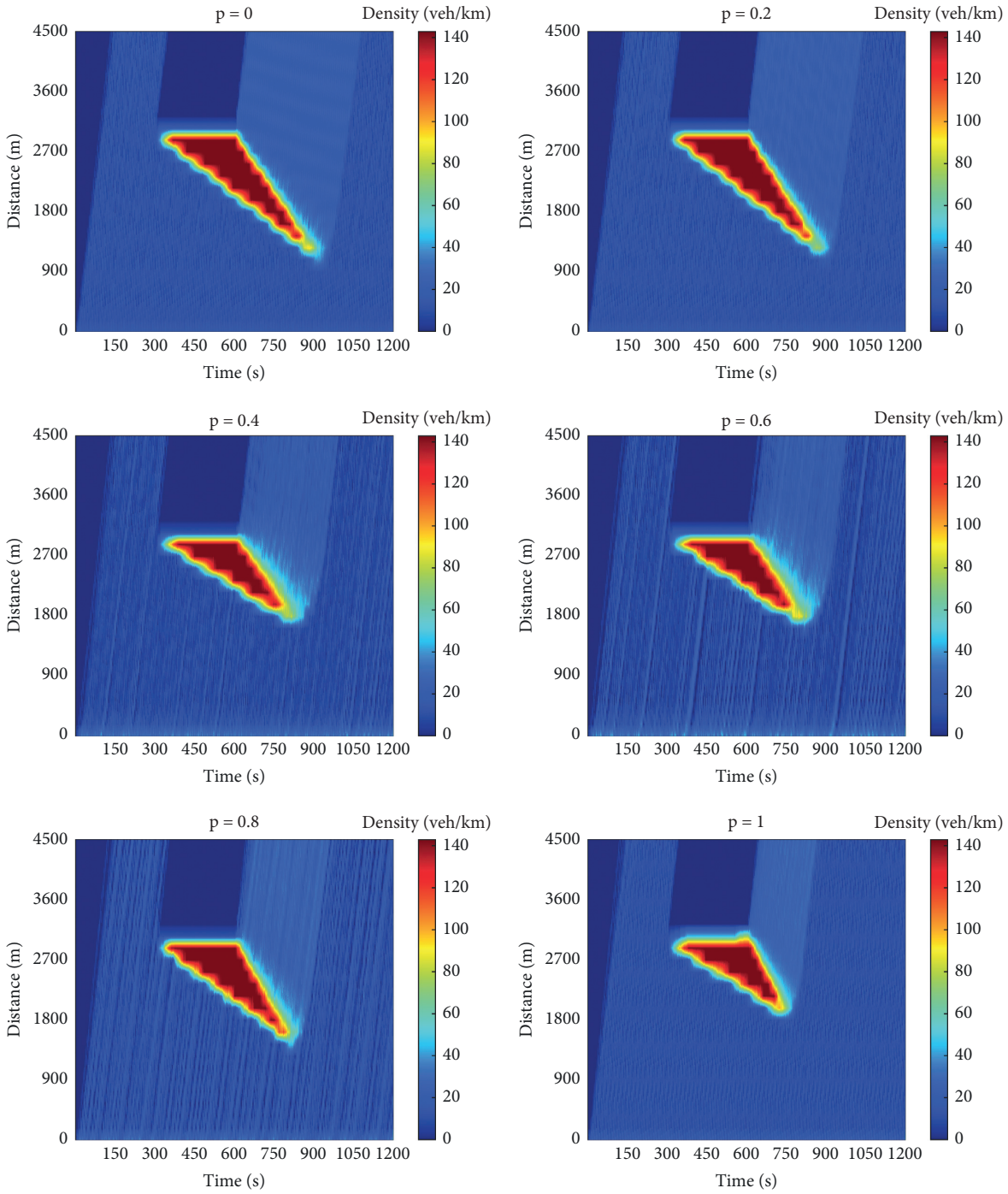

Figure 12: Density variation of micro-simulation.

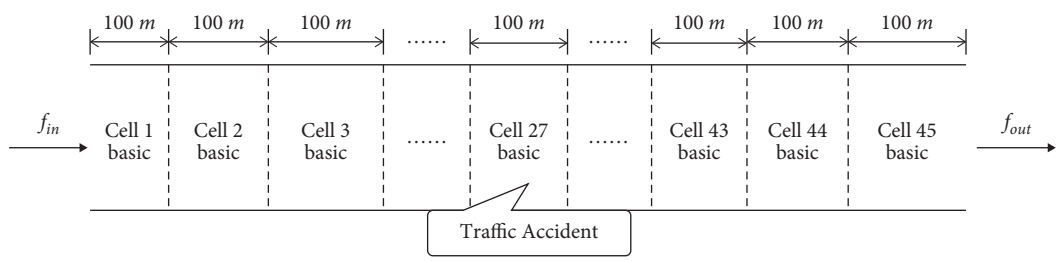

Figure 13: Mixed traffic flow simulation link.

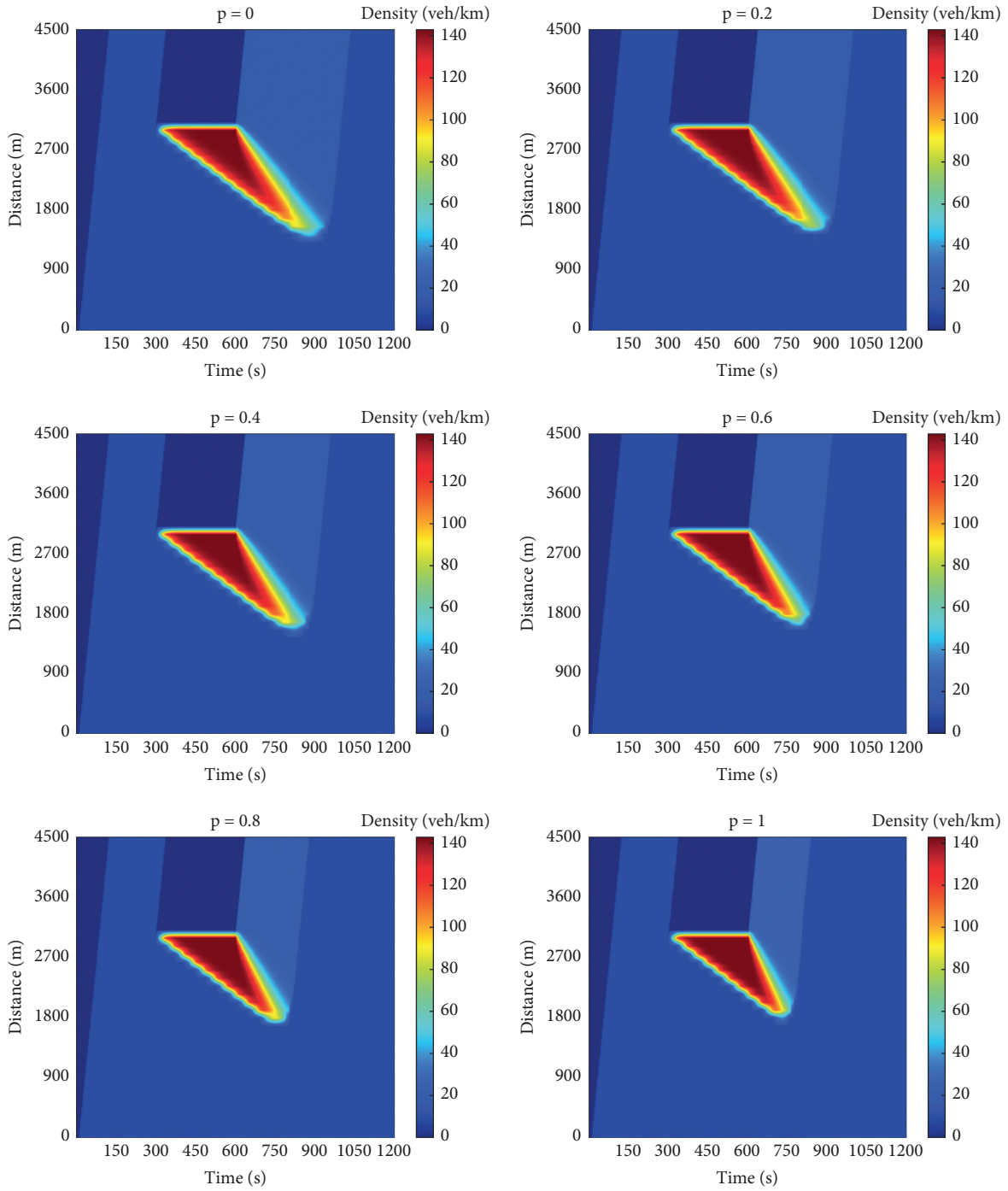

Figure 14: Density variation of CTM.

Table 2: Comparison of microscopic simulation, CTM, and VCTM.

p	Queue dissipation time (s)			MAE (s)		MAPE	
	Microscopic simulation	CTM	VCTM	CTM	VCTM	CTM	VCTM
0	919	906	912	13	7	1.41%	0.77%
0.2	895	888	897	7	2	0.78%	0.23%
0.4	844	849	846	5	2	0.59%	0.24%
0.6	834	816	831	18	3	2.16%	0.37%
0.8	814	780	792	34	22	4.18%	2.82%
1	746	753	741	7	5	0.94%	0.66%
Average	842	832	836.5	14	6.8	1.68%	0.83%

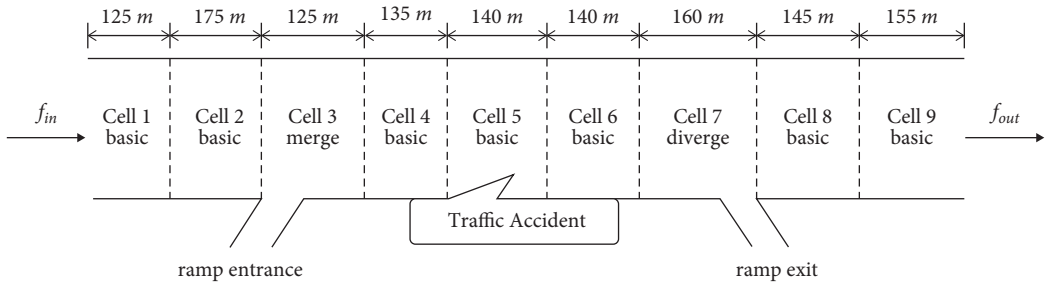

Figure 15: The simulation segment of mixed traffic flow.

In general, the simulation results of VCTM are closer to reality in the same simulation environment. Therefore, the VCTM can reflect the physical phenomena of queuing propagation and dissipation well. This is because the CTM needs to divide the research links into equal length cells for simulation experiment and does not consider the hysteresis phenomenon. On the contrary, the VCTM is proposed based on the improved three-phase traffic flow theory, which considers the substable region of the actual traffic flow in congestion. Therefore, the VCTM can analyze the whole evolution process of normal, congestion, and dissipation of unequal length segments. To sum up, the VCTM not only increases the flexibility of road traffic simulation but also make the simulation results more accurate and fit with the actual situation.

4. Analysis of Mixed Traffic Flow Characteristics

4.1. VCTM Simulation for Mixed Traffic Flow. The expressway with a basic link, merging link, and a diverging link is selected as the study road segment. The total length is 1300 m, and it is divided into nine cells with unequal lengths, as shown in Figure 15. Among them, the simulation step is 3 s, the free-flow speed is 33.3 m/s, the input flow is 1200 veh/h, the main road merging coefficient is 0.6, the ramp entrance is 0.4, the main road diverging coefficient is 0.7, and the ramp exit is 0.3. In addition, the traffic accident is set at 700 m section, and the duration is 300 to 600 s. To study the influence of the MPR of CAVs on physical phenomena, such as mixed traffic flow congestion and queuing, the MPR is set as 0, 0.2, 0.4, 0.6, 0.8, and 1.0, respectively. The numerical simulation experiment is carried out by MATLAB, and the change of cell flow with time on the road segments is obtained, as shown in Figure 16.

As shown in Figure 16, the traffic accidents occurred at 300 s, the traffic flow of each cell decreased rapidly, and the traffic volume reached the highest when the congestion began to dissipate. When $p = 1$, the maximum volume is 2975 veh/h, and the road capacity recovery time is 438 s. When $p = 0$, the maximum volume is only 2105 veh/h, and the road capacity recovery time is 501 s. The homogeneous CAVs traffic flow capacity can reach 1.41 times of the homogeneous HDVs traffic flow, and the congestion dissipation time can be reduced by 25%. The results show that with the increase of the MPR of CAVs, the road capacity increases gradually; that is, CAVs are conducive to improving the efficiency of the traffic system.

In addition, compared with the basic link, the traffic volume of the merging and diverging link has obvious changes. This indicates that the location of the ramp entrance and exit has a specific impact on the capacity of the expressway. The changing length of cells can make the road traffic layout more reasonable. Therefore, the VCTM can more accurately describe the mixed traffic flow characteristics of the expressway.

To understand the congestion dissipation mechanism of mixed traffic flow well, the VCTM simulation results are further analyzed.

4.2. Congestion Analysis. To further study the influence of the MPR of CAVs on the congestion dissipation capacity of the expressway, the VCTM is used to simulate the mixed traffic flow of Section 4.1. Then, the average travel speed, congestion delay, and congestion scale are combined to analyze and evaluate the road congestion dissipation capacity [49–52].

4.2.1. Average Travel Speed. The average travel speed refers to the average travel speed of all vehicles in the traffic network. It is an important index to evaluate road traffic smoothness. The calculation formula is as follows based on the cells.

$$v_i(t) = v_{\min} + \left(v_f - v_{\min}\right)\left[1 - \frac{k_i(t)}{k_j}\right], \tag{32}$$

where $v_{\min}$ is the minimum speed corresponding to congestion density (generally 13 km/h).

Figure 17 shows that the evolution law of traffic congestion and queue dissipation after the traffic accident of 300 s to 600 s at 700 m of the simulation section. At 300 s, vehicles in the fifth cellular began to queue and wait. The congestion spread forward the sequential cell. The average travel speed of the vehicles in the whole simulation road suddenly dropped below 5 m/s. When the traffic accident was cleared up at 600 s, the congestion began to dissipate, and the vehicles in each cell gradually recovered to normal driving speed. In addition, when the road is the homogeneous HDVs traffic flow, the vehicle speed recovery time needs 804 s after congestion dissipation. While the speed recovery time of the homogeneous CAVs traffic flow only needs 738 s. Therefore, the recovery time of speed is inversely related to the MPR of CAVs; that is, the greater MPR of

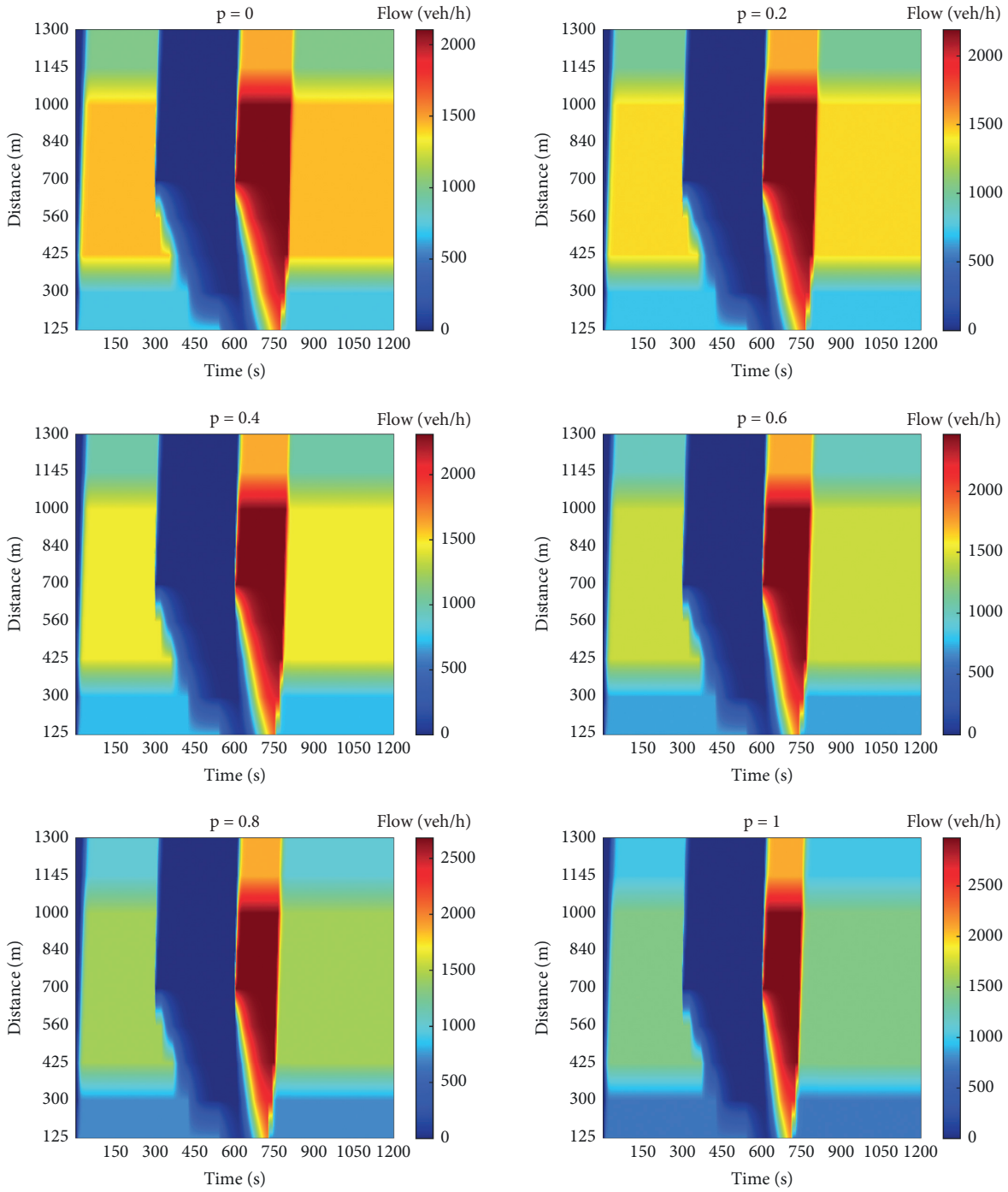

Figure 16: The variation of traffic flow based on VCTM.

CAVs, the shorter the recovery time of vehicle speed. This indicates that the CAVs traffic flow has a strong recovery ability after congestion evacuation, which is conducive to alleviating the traffic congestion and improving the efficiency of the traffic system.

4.2.2. Congestion Delay. Individual congestion delay refers to the difference between the number of vehicles in cell i and the number of vehicles leaving at time T. The overall congestion delay reflects the operation efficiency of the whole traffic system and the state of the road link at the beginning and end congestion. We assume the cell number is I, and the overall congestion delay is presented as

$$D = \sum_{i=1}^{I} \Delta t \left[n_i(t) - f_{i+1}(t) \right]. \tag{33}$$

Figure 18 shows that the road congestion and delay in the whole simulation period, where the cell number is 9. At 300 s, the congestion begins to spread from the fifth cell, and the delay of the whole road increases rapidly. The

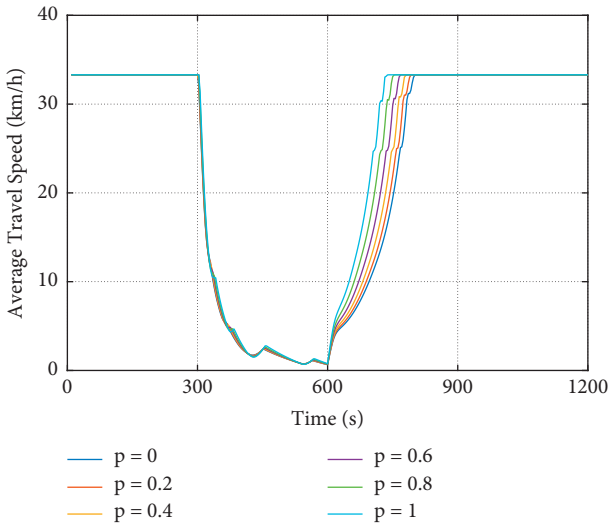

Figure 17: Average travel speed.

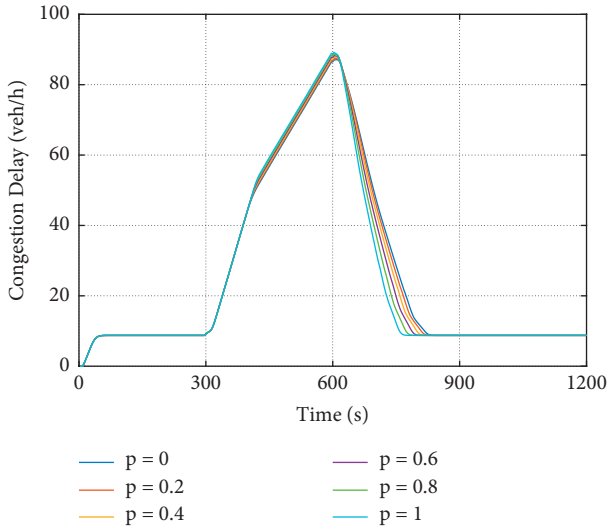

Figure 18: Congestion delay.

congestion begins to dissipate at 600 s, and the delay gradually decreases. In addition, the delay of traffic congestion gradually decreases with the increase of the MPR of CAVs. Therefore, the congestion delay is inversely proportional to the MPR of CAVs; that is, the higher the MPR is, the lower the congestion delay is, and the shorter the dissipation time is. This suggests that the large-scale application of CAVs is helpful to reduce traffic congestion and delay.

4.2.3. Congestion Scale. Congestion scale is the number of congested road segments to the total number of road segments in the traffic network. In the VCTM, it is the ratio of the number of congested cells to the total number of road cells. Therefore, the congestion scale is an important indicator reflecting the congestion situation and traffic capacity of the whole traffic network. Its calculation formula is as follows:

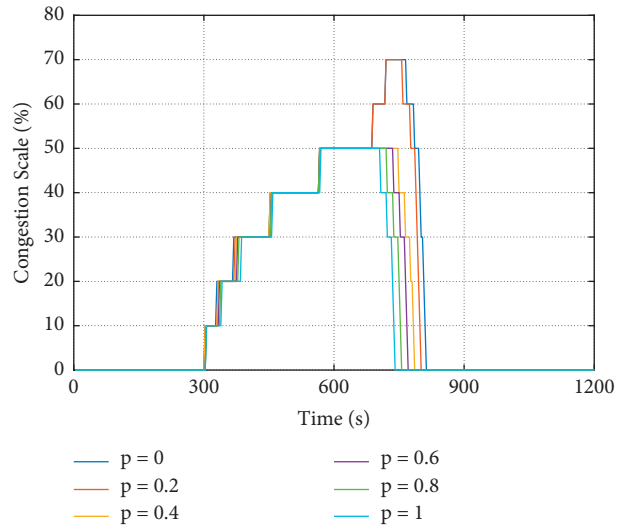

Figure 19: Congestion scale.

$$S = \frac{M_C}{M_T}, \tag{34}$$

where M_C is the number of congestion cells, and M_T is the total number of road cells.

Figure 19 shows the degree of traffic congestion in the simulation period. At 300 s, the number of congestion cells began to increase. The congestion began to dissipate at 600 s, and the number of congestion cells gradually decreased. In addition, when the traffic system is homogeneous HDVs traffic flow, the maximum congestion degree reaches 70%, while that of homogeneous CAVs traffic flow is only 50%. Therefore, the traffic congestion degree is inversely related to the MPR of CAVs. The greater the MPR, the lower the congestion degree. This indicates that the CAVs traffic flow has a strong ability to improve the traffic congestion after the traffic accident.

4.2.4. Results. The results of congestion analysis show that the congestion delay of mixed traffic flow decreases with the increase of the MPR of CAVs. The reason may be that the vehicle can make safe and efficient decisions on accelerating and decelerating in the CAVs environments [53]. Therefore, CAVs can reduce the congestion degree of the whole traffic system. In addition, the traffic capacity will not increase infinitely with the increase of the MPR of CAVs, which is related to the free-flow speed, the minimum safe distance, and the expected headway [29].

5. Conclusions and Future Work

This paper proposes a VCTM to analyze the characteristics of mixed traffic flow with CAVs and HDVs. Based on the simulation, the following conclusions can be drawn.

(1) The mixed traffic flow is proportional to the MPR of CAVs, that is, with the increase of the MPR, the capacity of the mixed traffic flow increases gradually.

The closer the MPR is to 1, the more significant the improvement effect on the traffic capacity is.

(2) Compared with the classical CTM, the VCTM can more accurately reflect the changes of traffic volume and density with time in different types of road sections (merging, diverging, and basic road links). The VCTM can clearly describe the physical phenomena of congestion and dissipation in each road segment.

(3) The results of congestion analysis show that the congestion delay of mixed traffic flow decreases with the increase of the MPR of CAVs.

This paper studies the characteristics of mixed traffic flow based on VCTM and draws some exciting conclusions. However, there are two regrets in this paper. First of all, we did not consider the influence of different headways, traffic demand, and ramp entrance and exit location on the characteristics of mixed traffic flow. In addition, we have not been extended the VCTM to the research of multiple lanes. Therefore, more deep research can be conducted from the following aspects in the future: (1) different factors will be introduced for sensitivity analysis, and the influence of different trajectory planning strategies of CAV on the characteristics of mixed traffic flow will also be studied. (2) The model is further extended to study multiple lanes of the expressway.

Data Availability

No data were used to support this study.

Conflicts of Interest

The authors declare that they have no conflicts of interest.

Acknowledgments

This paper received research funding support from the National Natural Science Foundation of China (52002339), the Sichuan Science and Technology Program (2021YJ0535), the Fundamental Research Funds for the Central Universities (2682021CX058), and the Guangxi Science and Technology Program (2021AA01007AA).

References

[1] Z. Yao, H. Jiang, Y. Cheng, Y. Jiang, and B. Ran, "Integrated schedule and trajectory optimization for connected automated vehicles in a conflict zone," *IEEE Transactions on Intelligent Transportation Systems*, vol. 23, no. 3, pp. 1841–1851, 2020.

[2] D. Jia and D. Ngoduy, "Platoon based cooperative driving model with consideration of realistic inter-vehicle communication," *Transportation Research Part C: Emerging Technologies*, vol. 68, pp. 245–264, 2016.

[3] D. Ngoduy, "Analytical studies on the instabilities of heterogeneous intelligent traffic flow," *Communications in Nonlinear Science and Numerical Simulation*, vol. 18, no. 10, pp. 2699–2706, 2013.

[4] W. Zhao, D. Ngoduy, S. Shepherd, R. Liu, and M. Papageorgiou, "A platoon based cooperative eco-driving model for mixed automated and human-driven vehicles at a signalised intersection," *Transportation Research Part C: Emerging Technologies*, vol. 95, pp. 802–821, 2018.

[5] M. Carey, "The cell transmission model with free-flow speeds varying over time or space," *Transportation Research Part B: Methodological*, vol. 147, 2021.

[6] X. Chen, Q. Shi, and L. Li, "Location specific cell transmission model for freeway traffic," *Tsinghua Science and Technology*, vol. 15, no. 4, pp. 475–480, 2010.

[7] R. Jiang, Q. S. Wu, and B. H. Wang, "Cellular automata model simulating traffic interactions between on-ramp and main road," *Phys. Rev. E.*, 2002.

[8] C. F. Daganzo, "The cell transmission model, part II: network traffic," *Transportation Research Part B: Methodological*, vol. 29, no. 2, pp. 79–93, 1995.

[9] C. F. Daganzo, "The cell transmission model: a dynamic representation of highway traffic consistent with the hydrodynamic theory," *Transportation Research Part B: Methodological*, vol. 28, no. 4, pp. 269–287, 1994.

[10] D. Ngoduy, "Noise-induced instability of a class of stochastic higher order continuum traffic models," *Transportation Research Part B: Methodological*, vol. 150, pp. 260–278, 2021.

[11] J. Long, Z. Gao, X. Zhao, A. Lian, and P. Orenstein, "Urban traffic jam simulation based on the cell transmission model," *Networks and Spatial Economics*, vol. 11, no. 1, pp. 43–64, 2011.

[12] A. Muralidharan and R. Horowitz, "Optimal control of freeway networks based on the Link Node Cell transmission model," in *Proceedings of the Am. Control Conf.*, IEEE, Montreal, QC, Canada, 27 June 2012.

[13] S. Timotheou, C. G. Panayiotou, and M. M. Polycarpou, "Distributed traffic signal control using the cell transmission model via the alternating direction method of multipliers," *IEEE Transactions on Intelligent Transportation Systems*, vol. 16, pp. 919–933, 2015.

[14] K. Tiaprasert, Y. Zhang, C. Aswakul, J. Jiao, and X. Ye, "Closed-form multiclass cell transmission model enhanced with overtaking, lane-changing, and first-in first-out properties," *Transportation Research Part C: Emerging Technologies*, vol. 85, pp. 86–110, 2017.

[15] W. Y. Szeto, B. Ghosh, B. Basu, and M. O'Mahony, "Multivariate traffic forecasting technique using cell transmission model and SARIMA model," *Journal of Transportation Engineering*, vol. 135, no. 9, pp. 658–667, 2009.

[16] C.-W. Carlos and A. Ferrara, "A variable-length cell road traffic model: application to ring road speed limit optimization," in *Proceedings of the 2016 IEEE 55th Conf. Decis. Control CDC*, pp. 6745–6752, IEEE, Las Vegas, NV, USA, 12 Dec. 2016.

[17] Z. Zhang, B. Wolshon, and V. V. Dixit, "Integration of a cell transmission model and macroscopic fundamental diagram: network aggregation for dynamic traffic models," *Transportation Research Part C: Emerging Technologies*, vol. 55, pp. 298–309, 2015.

[18] C. Shirke, A. Bhaskar, and E. Chung, "Macroscopic modelling of arterial traffic: an extension to the cell transmission model," *Transportation Research Part C: Emerging Technologies*, vol. 105, pp. 54–80, 2019.

[19] H. Dong, S. Ma, M. Guo, and D. Liu, "Research on analysis method of traffic congestion mechanism based on improved cell transmission model," *Discrete Dynamics in Nature and Society*, vol. 2012, pp. 1–11, 2012.

[20] G. Gomes and R. Horowitz, "Optimal freeway ramp metering using the asymmetric cell transmission model,"

Transportation Research Part C: Emerging Technologies, vol. 14, no. 4, pp. 244–262, 2006.

[21] G. Flötteröd and J. Rohde, "Operational macroscopic modeling of complex urban road intersections," *Transportation Research Part B: Methodological*, vol. 45, pp. 903–922, 2011.

[22] A. Srivastava, W.-L. Jin, and J.-P. Lebacque, "A modified Cell Transmission Model with realistic queue discharge features at signalized intersections," *Transportation Research Part B: Methodological*, vol. 81, pp. 302–315, 2015.

[23] Y. Gao, Y. Liu, H. Hu, and Y. Ge, "An enhanced cell transmission model for traffic operations within a signalized intersection," *Transp. Res. Board Annu. Meet.*, 2015.

[24] H. K. Lo, "A cell-based traffic control formulation: strategies and benefits of dynamic timing plans," *Transportation Science*, vol. 35, no. 2, pp. 148–164, 2001.

[25] W.-H. Lin and C. Wang, "An enhanced 0-1 mixed-integer LP formulation for traffic signal control," *IEEE Transactions on Intelligent Transportation Systems*, vol. 5, no. 4, pp. 238–245, 2004.

[26] L. C. Davis, "Nonlinear dynamics of autonomous vehicles with limits on acceleration," *Physica A: Statistical Mechanics and Its Applications*, vol. 405, pp. 128–139, 2014.

[27] S. E. Shladover, C. Nowakowski, X. Y. Lu, and R. Ferlis, "Cooperative adaptive cruise control (cacc) definitions and operating concepts," in *Proceedings of the 94th TRB Annu. Conf.*, January 2015.

[28] Z. Yao, R. Hu, Y. Jiang, and T. Xu, "Stability and safety evaluation of mixed traffic flow with connected automated vehicles on expressways," *Journal of Safety Research*, vol. 75, pp. 262–274, 2020.

[29] Z. Yao, R. Hu, Y. Wang, Y. Jiang, B. Ran, and Y. Chen, "Stability analysis and the fundamental diagram for mixed connected automated and human-driven vehicles," *Physica A: Statistical Mechanics and Its Applications*, vol. 533, Article ID 121931, 2019.

[30] M. W. Levin and S. D. Boyles, "A cell transmission model for dynamic lane reversal with autonomous vehicles," *Transportation Research Part C: Emerging Technologies*, vol. 68, pp. 126–143, 2016.

[31] Y. Qin and H. Wang, "Cell transmission model for mixed traffic flow with connected and autonomous vehicles," *Journal of Transportation Engineering, Part A: Systems*, vol. 145, no. 5, Article ID 04019014, 2019.

[32] Z. Yao, T. Xu, Y. Jiang, and R. Hu, "Linear stability analysis of heterogeneous traffic flow considering degradations of connected automated vehicles and reaction time," *Physica A: Statistical Mechanics and Its Applications*, vol. 561, Article ID 125218, 2021.

[33] A. Ghiasi, O. Hussain, Z. Qian, X. Li, and X. Li, "A mixed traffic capacity analysis and lane management model for connected automated vehicles: a Markov chain method," *Transportation Research Part B: Methodological*, vol. 106, pp. 266–292, 2017.

[34] C. Canudas-de-Wit and A. Ferrara, "A variable-length cell transmission model for road traffic systems," *Transportation Research Part C: Emerging Technologies*, vol. 97, pp. 428–455, 2018.

[35] M. Treiber, A. Kesting, and D. Helbing, "Influence of reaction times and anticipation on stability of vehicular traffic flow," *Transp. Res. Rec. J. Transp. Res. Board.*no. 2007, pp. 23–29, 1999.

[36] H. L. Yan and X. J. Liu, "Variable cell transmission model and simulation system design in consideration of hysteresis phenomena," *Internet Things Technol*, 2013.

[37] B. S. Kerner, "Three-phase traffic theory and highway capacity," *Physica A: Statistical Mechanics and Its Applications*, vol. 333, pp. 379–440, 2004.

[38] V. Punzo, M. T. Borzacchiello, and B. F. Ciuffo, "Estimation of vehicle trajectories from observed discrete positions and next-generation simulation Program (NGSIM) data," in *Transp. Res. Board Meet.*, 2009.

[39] E. N. Barmpounakis and N. Geroliminis, "On the new era of urban traffic monitoring with massive drone data: the pNEUMA large-scale field experiment," *Transportation Research Part C: Emerging Technologies*, vol. 111, pp. 5–71, 2020.

[40] R. Arvin, A. J. Khattak, M. Kamrani, and J. Rio-Torres, "Safety evaluation of connected and automated vehicles in mixed traffic with conventional vehicles at intersections," *J. Intell. Transp. Syst.*, pp. 1–18, 2020.

[41] Y. Yang, K. He, Y.-p. Wang, Z.-z. Yuan, Y.-h. Yin, and M.-z. Guo, "Identification of dynamic traffic crash risk for cross-area freeways based on statistical and machine learning methods," *Physica A: Statistical Mechanics and Its Applications*, vol. 595, Article ID 127083, 2022.

[42] X. Hu, W. Wang, and H. Sheng, "Urban traffic flow prediction with variable cell transmission model," *Journal of Transportation Systems Engineering and Information Technology*, vol. 10, no. 4, pp. 73–78, 2010.

[43] M. Treiber, A. Hennecke, and D. Helbing, "Congested traffic states in empirical observations and microscopic simulations," *Physical Review E*, vol. 62, no. 2, pp. 1805–1824, 2000.

[44] V. Milanés and S. E. Shladover, "Modeling cooperative and autonomous adaptive cruise control dynamic responses using experimental data," *Transportation Research Part C: Emerging Technologies*, vol. 48, pp. 285–300, 2014.

[45] V. Milanes, S. E. Shladover, J. Spring, C. Nowakowski, H. Kawazoe, and M. Nakamura, "Cooperative adaptive cruise control in real traffic situations," *IEEE Transactions on Intelligent Transportation Systems*, vol. 15, no. 1, pp. 296–305, 2014.

[46] H. Wang, Y. Qin, W. Wang, and J. Chen, "Stability of CACC-manual heterogeneous vehicular flow with partial CACC performance degrading," *Transp. B.*vol. 7, pp. 1–26, 2018.

[47] J. Chen, B. Yuan, and M. Tomizuka, "Deep imitation learning for autonomous driving in generic urban scenarios with enhanced safety," IEEE, 2019, https://arxiv.org/abs/1903.00640.

[48] G. Li, Z. Yang, Q. Yu, J. Ma, and S. Fang, "Characterizing heterogeneity among merging positions: a comparison study between random parameter and latent class accelerated hazardmodel," *Journal of Transportation Engineering*, vol. 147, 2021.

[49] M. Kuwahara and T. Akamatsu, "Decomposition of the reactive dynamic assignments with queues for a many-to-many origin-destination pattern," *Transportation Research Part B: Methodological*, vol. 31, no. 1, pp. 1–10, 1997.

[50] W.-X. Wang, R.-J. Guo, and J. Yu, "Research on road traffic congestion index based on comprehensive parameters: taking Dalian city as an example," *Advances in Mechanical Engineering*, vol. 10, no. 6, 2018.

[51] F. V. Webster, "Traffic signal settings," *Road Res. Tech. Pap.*vol. 39, 1958.

[52] C. Wright and P. Roberg, "The conceptual structure of traffic jams," *Transport Policy*, vol. 5, no. 1, pp. 23–35, 1998.

[53] X. Hu, M. Huang, and J. Guo, "Feature analysis on mixed traffic flow of manually driven and autonomous vehicles based on cellular automata," *Mathematical Problems in Engineering*, vol. 2020, pp. 1–7, 2020.